Broadband extrinsic self-trapped exciton emission in Sn-doped 2D lead-halide perovskites

Yu, Jiancan; Kong, Jintao; Hao, Wei; Guo, Xintong; He, Huajun; Leow, Wan Ru; Liu, Zhiyuan; Cai, Pingqiang; Qian, Guodong; Li, Shuzhou; Chen, Xueyuan; Chen, Xiaodong

2019

Yu, J., Kong, J., Hao, W., Guo, X., He, H., Leow, W. R., . . . Chen, X. (2018). Broadband Extrinsic Self-Trapped Exciton Emission in Sn-Doped 2D Lead-Halide Perovskites. Advanced Materials, 31(7), 1806385-. doi:10.1002/adma.201806385

https://hdl.handle.net/10356/144533

https://doi.org/10.1002/adma.201806385

DOI: 10.1002/((please add manuscript number))
Article type: Communication

Broadband Extrinsic Self-trapped Exciton Emission in Sn-doped 2-Dimensional Lead-halide Perovskites

Jiancan Yu,‡ Jintao Kong,‡ Wei Hao,‡ Xintong Guo, Huajun He, Wan Ru Leow, Zhiyuan Liu, Pingqiang Cai, Guodong Qian, Shuzhou Li, Xueyuan Chen, and Xiaodong Chen**

Dr. J. Yu, Dr. W. Hao, Ms X. Guo, Dr. W. R. Leow, Dr. Z. Liu, Dr. P. Cai, Prof. Dr. S. Li, Prof. Dr. X. Chen
Innovative Centre for Flexible Devices (iFLEX), School of Materials Science and Engineering, Nanyang Technological University Singapore, 639798, Singapore
E-mail: chenxd@ntu.edu.sg

Dr. J. Kong, Prof. Dr. X. Chen
CAS Key Laboratory of Design and Assembly of Functional Nanostructures, Fujian Key Laboratory of Nanomaterials, Fujian Institute of Research on the Structure of Matter, Chinese Academy of Sciences, Fuzhou, Fujian 350002, China
E-mail: xchen@fjirsm.ac.cn

Mr. H. He, Prof. Dr. G. Qian
State Key Laboratory of Silicon Materials, School of Materials Science and Engineering, Zhejiang University, Hangzhou 310027, China

‡ These authors contributed equally to this work.

Keywords: perovskites, Sn-doping, self-trapped excitons, luminescence, extrinsic

Abstract: As emerging efficient emitters, metal-halide perovskites offer the intriguing potential to the low-cost light emitting devices. However, semiconductors generally suffer from severe luminescence quenching due to insufficient confinement of excitons (bound electron-hole pairs). Here, we report Sn-triggered extrinsic self-trapping of excitons in bulk 2-dimensional perovskite crystal, PEA_2PbI_4 (PEA = phenylethylammonium), where exciton self-trapping never occurs in its pure state. By creating local potential wells, isoelectronic Sn dopants initiate the localization of excitons, which would further induce the large lattice deformation around the impurities to accommodate the self-trapped excitons. With such self-trapped states, the Sn-doped perovskites generate broadband red to near-infrared (NIR) emission at room temperature due to strong exciton-phonon coupling, with a remarkable quantum yields increase from 0.7% to 6.0% (8.6 folds), reaching 42.3% under a 100-mW/cm^2 excitation by extrapolation. The quantum yield enhancement stems from substantial higher thermal quench activation energy of self-trapped excitons than that of free excitons (120 vs 35 meV). We further revealed that the fast exciton diffusion involves in the initial energy transfer step by transient absorption spectroscopy. This dopants-induced extrinsic exciton self-trapping approach paves the way for extending the spectral range of perovskite emitters, and may find emerging application in efficient supercontinuum sources.

Metal-halide perovskites represent a class of promising light absorbers for efficient solar cells.[1-5] The propensity of perovskite films for low-cost solution processing also encourages scientists to explore potential applications beyond solar cells.[6-9] In particular, as emitters, perovskites exhibit intriguing luminescent properties such as narrowband emission, spectral tunability, and high quantum efficiency, which enables applications in the micro-lasers and light-emitting diodes (LEDs).[10-13] The luminescence efficiency of perovskites generally relies on nanostructures that can spatially confine excitons, and consequently reduce the possibility of non-radiative recombination during the carrier/exciton migration. However, nanocrystals, due to boundary scattering of carriers, generally face the problem of poor charge transport, which is undesirable for LED performance. 2-Dimensional (2D) perovskites, where bulky organic layers and inorganic layers are alternately and periodically arranged, feature natural quantum-well structures. This quantum-well structure is regarded as promising LED emitters for decades.[14-16] However, low photoluminescence quantum yields (PLQYs, typically <1%) of 2D perovskites at room temperature is a bottleneck to achieving high-performance LEDs.[17] The low PLQYs may be attributed to insufficient confinement of Wannier type excitons within the inorganic layers[18] as suggested by the long charge-carrier/exciton diffusion length (60 nm).[19]

Engineering crystal structures of low-dimensional (0D to 2D) perovskites by employing suitable organic ammonium cations is the predominant methods for the tuning of luminescence, both in spectral coverage and efficiency.[20, 21] In these cases,

severe structural distortion of metal halide octahedra is a common feature because of the size mismatch between organic and inorganic components, which results in potential fluctuations.[22, 23] Such fluctuations of potential within an inorganic layer of perovskite sometimes, but not always,[20, 21] slow the diffusion of carriers or excitons, and consequently induce self-trapped excitons (STEs), which represents a type of bound states for efficient radiative recombination. However, the occurrence of exciton self-trapping in semiconductors is the exception rather than the rule.[24] In parallel, compositional engineering of perovskites, such as doping and alloying, also shows the capability to route and confine excitons around the dopants for radiative recombination, and thus improve PLQYs of the resulting emitters.[24] However, color tunability and PLQY improvement were typically achieved only in nanostructures,[25] including inorganic perovskite nanocrystals,[26-31] probably due to the low doping limit that is not sufficient to compensate for the abundant defects in bulk. Fortunately, similar electron structures and radii of Sn with Pb cations allow the doping or alloying of Sn in Pb-based perovskites readily, without doping limit.[32-34] But slightly Sn doping fails to remarkably tune the PL properties in 3-dimensional (3D) perovskites yet,[28, 32, 35] since Sn doping only narrows the band gap slightly and band-edge emission dominates in these 3D perovskites. In fact, exciton localization and polaronic effect are presumably present in 3D perovskites,[36, 37] but they are so weak to further confine excitons as trapped states. In low-dimension perovskites where excitons show the tendency of self-trapping, intentional doping provides a new opportunity for facilitating exciton self-trapping. It is coined as extrinsic self-trapping,

which has succeeded in II-VI alloys (e.g. $ZnSe_{1-x}Te_x$, $x \approx 0.01$) at low temperature,[38, 39] but not yet reported in lead-halide perovskites to the best of our knowledge.

Herein, we report Sn-induced self-trapped excitons in 2D perovskite PEA_2PbI_4 (PEA = phenylethylammonium), which offer broadband extrinsic red-to-near-infrared (NIR) luminescence with enhanced PLQYs at room temperature. Unlike several low-dimensional perovskites that afford broadband emission from STEs,[40] pure 2D perovskite PEA_2PbI_4 only shows narrowband emission from free and bound excitons even at low temperature. Interestingly, a trace amount of Sn dopants (as low as 0.00005%) in the 2D perovskite induces a remarkable broadband luminescence ranging from red to NIR region. The emerging broadband emission assigned to extrinsic STEs arises from the interplay of impurity-driven exciton accumulation and the strong exciton-phonon coupling. Excitons are localized loosely as a compromise of Wannier exciton feature in the inorganic layers[18] and dopants-induced potential wells. Such strong coupling is endowed by the polar nature of metal-halide perovskites. The Sn-triggered exciton localization through fast exciton diffusion (< 1 ps) is revealed by transient absorption (TA) spectroscopy. This ubiquitous energy transfer pathway in semiconductors of such high binding energy is independent on the carrier migration, and offers an additional efficient exciton relaxation pathway that suppresses inefficient free and bound exciton emission. As a result, PLQY values are improved from 0.7% to 6.0% (~8.6 folds), which can reach 42.3%, when the excitation density is extrapolated to a modest value of 100 mW/cm^2. This doping

strategy in bulk 2D perovskite crystals provides an approach to the control of exciton dynamics, and consequently tune the emission spectra and optimize PLQYs.

PEA_2PbI_4 and Sn-doped perovskite crystals were synthesized under solvothermal condition using acetonitrile and hydroiodic acid as solvents (see details in Supporting Information). We were able to prepare the solid solution of PEA_2PbI_4:Sn(X) (where X refers to the measured fraction of Sn in the compounds) with high tunability of the doping levels. Unlimited solid solubility comes from their structural similarity that both PEA_2PbI_4 and its Sn-counterpart, PEA_2SnI_4, share the same phase with only slight differences in cell parameters (<1%, see Table S1).[14, 41] It should be noted that the inert gas atmosphere is necessary to prevent the oxidization of Sn^{2+} during preparation. Otherwise, Sn atoms would be excluded from the crystal lattices, since the effective ionic radius of Sn^{4+} (69.0 pm for the 6-coordination) is much smaller than that of the Sn^{2+} and Pb^{2+} cations (118 pm and 119 pm, respectively).[42] Powder XRD patterns reveal that Sn-doped 2D perovskites retain the phase (Figure S1). Inductively coupled plasma mass spectrometry (ICP-MS) reveals that the amounts of incorporated Sn dopants in Sn-doped perovskites were around half of the nominal values, presumably due to the slight difference in reaction kinetics and energetics. However, the doping levels calculated from ICP-MS results only reflect the averaged amount of Sn, and there might be doping level difference between individual crystals. But within a crystal, the distribution of Sn seems homogeneous on the microscopic scale; we could not observe localized red spot under a microscope (Figure S2; lens magnification, 50×), even at low excitation power. The

elemental mapping using energy-dispersive X-ray spectroscopy and confocal luminescence imaging further indicate the homogeneity of Sn distribution (Figure S3-4).

The luminescence properties of 2D perovskites, PEA_2PbI_4 and PEA_2SnI_4, have been explored for decades because of their unique quantum-well structures.[20, 41, 43-48] As a semiconductor of large binding energy (220 meV [43]), the luminescence of PEA_2PbI_4 is determined by the dynamics of excitons confined in the inorganic layer, as shown in **Figure 1**a and S5. PEA_2PbI_4 crystals generate green emission under ultra-violet or blue light excitation, with a spectral center at 525 nm, due to the recombination of free excitons in the 2D perovskite (Figure 1b and d).[46, 47] With 0.36%-Sn doping in the 2D perovskite, a bright broad red-to-NIR emission band was observed with a full width at half maximum (FWHM) of ~180 nm at the center of ~710 nm, while the original green emission almost disappears (Figure 1c and d). It is noteworthy that the peak of Sn-doped perovskite does not emerge between the emission peaks of pure PEA_2PbI_4 and PEA_2SnI_4 (625 nm), radically different from conventional semiconductor alloys whose emission peaks is located between those of two pure counterparts.[49] Such anomalous red-shifted luminescence observed in the Sn-doped 2D perovskite have not been observed in the Sn-alloyed 3D cases,[50] where band-edge emission always dominates.

We further investigated the influence of doping level on the PL properties. The green emissions at 525 nm due to the free exciton of PEA_2PbI_4 host decrease monotonically as the doping level of Sn increases, while the broad emissions induced

by Sn dopants increase first and then decrease after the doping level reaches 0.36% (Figure 2a-b). The PL intensity increases with doping levels at low content can simply attribute to a Sn-related photophysical process that leads to such broadband emission. The presence of optimal doping level suggests that such process is inhibited once Sn dopants reach a threshold value. We will later discuss the role of Sn dopants in giving rise to such emission. Besides, a shoulder peak at around 555 nm is also dwarfed as the doping level increase. This shoulder peak, which was frequently observed at low temperature but rarely found at room temperature, can be assigned to the emission from the bound excitons,[45, 47, 48, 51] although still being under debate.[52] PEA_2PbI_4 crystals show a low QY value of 0.7% (approaching the detection limit of the instrument) at room temperature (Figure 2c). With Sn doping, the best QY value of 2D perovskites raises to 6.0%, which is about 8.6 folds of the pristine one. It should be noted that the PLQYs were measured under a very low excitation density of ~80 $\mu W/cm^2$, and the superlinear emission increase with excitation density indicates that the PLQYs of Sn-doped perovskites should be much larger under a higher light fluence (Figure 2d).[53] Although the superlinear power law become invalid at a high excitation fluence (~20 mW/cm^2, see Figure S6), beyond which condition the emission may partly be limited by the dopant concentration and the risk of non-radiative Auger processes,[53] the PLQY of 0.36%-Sn doped sample keeps increasing until the slope reaches 1. Consequently, the estimated PLQY values reach 25.5% and 42.3%, respectively, under a modest excitation density of 10 and 100 mW/cm^2, assuming the absorption coefficient keeps constant. In contrast, the PLQY of pristine

perovskite, PEA_2PbI_4, remains a low value of 0.7%, as its PL intensity increases linearly with the excitation fluence.

As for the origin of unusual broad emission peaks of Sn-doped 2D perovskites, we can easily exclude the possibility of inhomogeneous aggregation of SnI_6 units. First, the pure Sn-based 2D perovskite generates narrowband emission at ~625 nm, and their aggregates should emit at a blue-shifted region according to the fundamental quantum size effect. Second, in the dilute case (doping level of 0.00005%), where another 1410 Pb atoms separate an Sn atom in average, the FWHM of its emission spectrum still reaches 170 nm, similar to samples of higher doping levels. Furthermore, a similar PL decay of Sn-doped perovskites suggests that the emission across a wide range has the same mechanism (Figure S7), rather than from different SnI_6 aggregates. In fact, no characteristic excitonic peak of PEA_2SnI_4 was observed in the UV-vis spectra even when the molar ratio of Sn/(Sn+Pb) reaches 20% (Figure S8), suggesting the absence of phase separation or nanometer-size PEA_2SnI_4 precipitation in bulk crystals.

Self-trapped states in strong exciton-phonon coupled systems are the main sources responsible for broadband emissions, particularly in polar semiconductors. Broadband white-light emissions were occasionally observed in the low-dimensional hybrid perovskites, which are exclusively assigned to STEs.[23, 54, 55] The presence of STEs is typically elusive because of their transient quasi-particle feature; they manifest themselves through a broadband luminescence. Similarly, our Sn-doped perovskites show all the feature of STE emission, large Stokes' shift (~670 meV) and

smooth broadband emission spectra. Therefore, we can interpret such anomalous luminescence as extrinsic STEs emission, similar to the cases of II-VI semiconductor alloys.[38, 56] The formation of STEs requires two criteria: a strong electron-phonon coupling and excitons of the nature between Frenkel and Wannier type. First, in the 2D perovskites, exciton states can be regarded as Wannier type (delocalized) in the inorganic layer but of Frenkel type (localized) across the layers.[18] The presence of Sn dopants creates fluctuations of random potentials, localizing excitons behaving like weakly bounded excitons of Frenkel type. Second, strong exciton-phonon (electron-phonon) coupling is widely reported in 2D lead-halide perovskites, which contributes to the spectral broadening significantly.[21, 57] To quantify the exciton-phonon interaction and the inhomogeneous line width due to structural fluctuations, we estimated the upper limit of homopolar phonon deformation potential (D_{CV}) by simply ignoring the contribution of acoustic phonon to the FWHM of PL spectra (**Figure 3**).[57] The phonon-independent inhomogeneous line widths were fitted to be 209 and 218 meV, respectively, for 0.0053% and 0.36%-Sn doped perovskite crystals. These broad line widths suggest severe potential fluctuations around Sn dopants and relatively loose confinement of excitons nearby. The slightly wider line of 0.36%-Sn doped crystals than that of lower doping level may attribute to the larger lattice deformation around impurity at a higher doping level. These two samples also exhibit similar deformation potentials of 7.1 and 6.6 $\times 10^8$ eV/cm, respectively, for samples of 0.0053% and 0.36% Sn dopants, approximating to that in another 2D perovskite,

$(C_4H_9NH_3)_2PbI_4$.[57] The similarity in deformation potentials indicates that the doping of Sn actually has negligible effects on the interaction of the excitons with phonons.

As mentioned above, the role of Sn in triggering exciton self-trapping can be simply regarded as generating random potential wells. We chose Sn as a dopant for the Pb-based perovskites mainly due to its favorable electronic structure. The 5p orbits of Sn (-3.9 eV), which contribute dominantly to the conduction band minimum, are lower than the 6p orbits of Pb (-3.7 eV).[58, 59] To reveal the doping effect on the electronic properties of the resulting perovskites, we further performed density functional theory (DFT) calculation based on the Heyd-Scuseria-Ernzerhof (HSE) method. As shown in Figure S9, with Sn-doping, the valence band maxima of the resulting perovskites are retained, while the conduction band minima are shifted to lower energy levels. The magnitude of the shift increases as the doping levels increase. Besides, the Pb atoms and Sn dopant contribute to the conduction band minimum differently in the Sn-doped 2D perovskite (Figure S10); Sn dopants show the higher projected density of states than those of surrounding Pb atoms near the conduction band edge, and their contribution decreases at regions further away from the Sn dopant. This energy profile difference would form the basis for exciton localization by pushing the excitonic level to a low-lying energy level around the Sn dopant. In this way, subtle potential wells created by isoelectronic Sn dopants endow the impurities with the capacity to localize excitons around them, and the resulting bound excitons would further induce lattice deformation, consequently resulting in the strong exciton-phonon coupling.

To clarify the negligible role of intrinsically bound excitons in exciton self-trapping and improving luminescence efficiency, we revisited their temperature-dependent PL properties. Emission both from free and bound excitons increases as the temperature decreases (**Figure 4**a and S11), while the bound exciton emission increases more dramatically with a blue shift. Meanwhile, another peak emerges at around 545 nm with significantly higher intensity than that of the free excitons, resulting in an increase of PL integrated intensity by 28.7 folds. Notably, the bound exciton emission strongly depends on temperature; such emission weighs 93% of the whole spectrum at 25 K, but was severely quenched at room temperature. The continuous spectral evolution can exclude the phase transition during 25-300 K, similar to previous results of perovskite films.[46, 47] Based on temperature-dependent PL, we can extract the thermal activation energy for overall emissions from both free and bound excitons (Figure 4b-c). It is only 35 meV, approximating to the thermal energy k_BT at room temperature (26 meV), where k_B is Boltzmann constant. It should distinguish the thermal activation energy from binding energy. The former refers to the overall energy barrier for excitons to be bound to non-radiative defects, while the latter is relevant to exciton dissociation. Such low thermal activation energy can be explained for the difficulty in exciton localization at ambient temperature for efficient bound and self-trapped exciton emission. The failure in exciton localization mainly attributes to the unique feature of excitons in the 2D perovskites, where the exciton states can be regarded as Wannier type (delocalized) in inorganic layer, but of Frenkel

type (localized) across the layers.[18] This understanding of excitons in the shape of circular disk also well agrees with large diffuse length (60 nm) reported previously.[19]

In the pure perovskites, the nature of these bound states is still under debate,[45, 47, 48, 51] with a probable origin being the defects, mainly organic vacancies, which are located at the interface between inorganic and organic layers.[47, 51, 60] There is no clear evidence that the organic defects generate localized STE states (see PL spectra at 25 K, Figure S11). Even though organic vacancies possibly produce STE states, presumably much lower density of vacancies than the Sn-doped samples makes their role negligible. Therefore, bound excitons emission, although represents an efficient radiative channel, only weighs a small portion of the whole luminescence in this 2D perovskite at room temperature. On the contrary, doping presents a controllable way to tune the density of defects, especially for alloying types where there is no doping limit. Take the sample of highest PLQY (0.36% Sn) as an example, the areal density of Sn dopants reaches a considerable value of 3.8×10^{12} cm^{-2}, an inconceivably high concentration for intrinsic defects that may destroy the crystallinity of semiconductors.). However, at a high doping level (>~0.36%), Sn dopants have the trend of aggregation, which was implied by the blueshift of emission peak and emerging of characteristic emission of PEA_2SnI_4 at 625 nm (Figure 2b and Figure S14) once the doping level reaches 5%. In this case, the energy difference that Sn dopants impose is not sufficient to localize excitons efficiently so that self-trapping of excitons would not take place, and consequently both the PL intensity and PLQYs decrease dramatically.

As manifested in the emission spectra (Figure 2a), Sn dopants suppress the emission of bound excitons. The relative emission intensity of bound excitons (around 555 nm) to free excitons (525 nm) decreases with increasing doping levels. Notably, even at a low temperature of 25 K, PEA_2PbI_4:Sn(0.36%) shows very weak emission from bound excitons, while the undoped perovskite exhibits highly dominated bound exciton emission (Figure 4a). Compared with the intrinsic defects relevant to bound excitons, Sn dopants are abundant, abridging the diffusion length of excitons or carriers, and therefore taking less risk of non-radiative recombination during diffusion. Once STEs form, the thermal activation energy for this PL quench (120 meV) is substantially larger than that of undoped counterparts (35 meV, Figure 4b). These results clearly indicate that the emissions due to free and bound excitons are suppressed by foreign dopants which offer more efficient luminescence.

The exciton trapping is a process of energy transfer; the efficiency of the emission due to trapped exciton relies on the energy transfer kinetics. We have gained spectral clues of energy transfer, from luminescence spectral evolution of 2D perovskites upon Sn doping, PLQY enhancement, to dominant self-trapping exciton emission in low doping samples. In particular, a trace amount of Sn, e.g. PEA_2PbI_4:Sn(0.00005%), where an Sn dopant is surrounded by Pb atoms in a 1.8×10^4-nm^2 region, could render the Sn-induced emission dominant (68% in integral, Figure S12) with a doubled PLQY value. The increased PLQY value suggests that the red-to-NIR emission is from intimate energy transfer, rather than from the reabsorption and re-excitation events. For 0.36%-Sn sample, a Sn dopant occupies an

average area of 2633 $Å^2$, equivalent to a radius of 29 Å. This value is a little larger than the reported exciton Bohr radius of PEA_2PbI_4 (17 Å).[43] The feasibility to trap the excitons of PEA_2PbI_4 mainly stems from the potential wells, as well as the capability of exciton diffusion in the inorganic layers.[19, 61] In fact, the effective radius of Sn dopant to trigger STEs should be larger than 29 Å as the 0.0053%-Sn sample show a little drop in PLQY. Importantly, this PLQY value shows a sign of excitation power dependence, as suggested by the superlinear increase of STE emission with excitations fluence (Figure 2d and S13

To explore the kinetics of energy transfer, we investigated the transient PL properties. With Sn doping, the average PL lifetimes of free exciton exhibit a decreasing trend (Figure S15 and Table S2). For example, the averaged PL lifetimes drop from 1.00 to 0.28 ns after 5.0%-Sn doping. The shortened PL lifetime indicates the presence of a new exciton relaxation pathway, namely energy transfer. The fast PL lifetimes at the sub-nanosecond scale suggest that the following energy transfer should complete in the sub-nanosecond scale to survive severe PL quench and to give the self-trapped exciton emission in time. Then we tracked the PL decay of self-trapped states in PEA_2PbI_4:Sn(0.36%). These states are immediately populated and recombined radiatively upon the arrival of the excitation pulse without a resolved delay (**Figure 5**a). The delay remains negligible even for a 0.00005%-Sn-doped sample, indicating a fast energy transfer process from light absorption to ultimate radiation.

Figure 5b summarizes the relaxation channels of charge carriers and excitons in the excited Sn-doped 2D perovskites. Charge carrier migration (Pathway I) within the conduction band represents a fast energy transfer pathway. However it generally relaxes to excitons in a short period (10-50 fs).[47] For a quantum confined system with high binding energy, carriers relax to excitons almost irreversibly. Once the free carriers degenerated to excitons, the following process is governed by the kinetics of excitons. In this sense, long-range exciton diffusion (Pathway II), which may involve partial dissociation of excitons because of the presence of potential gradient posed by Sn dopants, is essential.

To reveal the energy transfer pathway, we firstly investigated the kinetics of exciton relaxation by the transient absorption techniques. 2D perovskite, PEA_2PbI_4, shows strong excitonic absorption centered at 516 nm. The excitonic peak remains remarkable upon 5% Sn doping, with a slight broadening to the low-energy side (Figure S8). The spectral broadening indicates the inhomogeneous broadening of excitonic levels, especially at the lower energy regions correlating to Sn-induced traps. Figure 5c-d show TA signals recorded with a 495-nm femtosecond pulse as the excitation source, the photon energy of which is insufficient for band-to-band transition (E_g = 2.58 eV,[43] corresponding to 481 nm). This condition excludes the relaxation of excited states related to charge carriers. PEA_2PbI_4 exhibits a narrow negative TA signal region centered around 516 nm, which is consistent with the excitonic absorption peak, and therefore can be attributed to exciton bleaching (XB). Compared to the pristine perovskite, the 5% Sn-doped film shows less bleaching at

516 nm, but additional negative signals at around 535 nm, which is consistent with the steady absorption. The weak bleaching at the lower energy side (~540 nm) can be assigned to the isoelectric traps induced by the Sn dopants.[24]

The whole TA spectra of pristine perovskite can be regarded as the overlap of three components, one from pronounced exciton bleaching and two from photoinduced absorption (PIA), as fitted in Figure S16. The kinetic traces of bleaching recovery at 516 nm for the pristine and Sn-doped films, which represent the kinetics of exciton relaxation, were fitted in a bi-exponential decay model, as shown in Figure 5e (see the details in Supporting Information). Different from the undoped film, ΔA of Sn-doped film recovers ~70% rapidly with a time constant of 0.85 ps, corresponding to fast energy transfer through Sn-oriented exciton diffusion from the PEA_2PbI_4 host to the Sn dopants. The small portion (25.5%) of the slow process (~0.18 ns) is probably associated with radiative and non-radiative recombination relevant to free excitons of perovskite host. This value is roughly consistent with the PL lifetime of free excitons mentioned above (0.28 ns). The time discrepancy is mainly due to the different excitation sources. The bleaching at the lower-energy side, which reflects the relaxation of Sn-induced trap states that is partly counteracted by PIA signals, reaches its minimum with only a ~1 ps delay, suggesting that excitons are transferred and trapped rapidly.

Next, we evaluated the carrier migration as another possible energy transfer pathway. This relaxation kinetics of carriers can be derived from TA kinetic profile through above-bandgap pumping (at 425 nm, Figure S17). Similarly, the remarkable

bleaching, which corresponds to the XB, was observed around 516 nm for Sn-doped films. Almost fixed XB peak with respect to undoped one shows the little contribution of carrier migration to energy transfer. Otherwise, XB band would inhomogeneously extend to the bathochromic-shift region, because part carriers would relax to an exciton of lower energy than that of the intrinsic one during impurity-directed migration. In fact, the energy transfer efficiency almost remains constant for both below and above bandgap excitation, as the weight of Sn-induced emission remains (Figure S12 and 18). The dominant Sn-triggered emission under sub-bandgap excitation (Figure S18) also indicates the essential role of exciton diffusion in energy transfer for 2D perovskites, which, to the best of our knowledge, was not emphasized before. It should be noted that, as a pathway of energy transfer, exciton diffusion is allowed in all semiconductors no matter how high the binding energy is, while carrier migrates readily only in semiconductors of low binding energy.

Self-trapping of excitons is detrimental to the efficiency of solar cells, but desired for efficient luminescence. It frequently occurs in conventional II-VI and I-VII semiconductors,[39] but was not observed unambiguously in ionic 3D lead-halide perovskites which are also highly polar in nature.[37] There is no doubt that the basic building block metal-halide octahedra are deformable, and the formation of STEs depends on the critical potential barriers which are related to the dimensionality of systems. By using the quantum mechanical treatment of a square well of various dimensions, it is deduced that a bound state appears only if the product V_0a^2 exceeds a

threshold value, where V_0 and a are the depth and width of the well, respectively.[39] This criterion leads to the conclusion that a minimum distortion is needed to create a sufficient well in 3 dimensions, and therefore a potential barrier that must be overcome to initiate self-trapping, whereas in quasi-one-dimensional systems there is no barrier to self-trapping.[39] This dimensional dependence suggests the difficulty in self-trapping in 3D perovskites and the feasibility in low-dimensional systems. Due to the challenge in creating a sufficient potential well by intrinsic materials themselves, a foreign shallow defect potentially provides the possibility of trapping free carriers or excitons cooperatively. In our case, Sn dopants exactly play such a role in assisting the exciton trapping. They serve like electron acceptors because of their low-lying energy level with respect to the orbit of Pb, and possibly positive charging due to partial oxidation, as evident in the Sn3d XPS signals that is broadened to the larger binding energy in Sn-doped perovskites with respect to the pure Sn-based one (Figure S19). In this way, partially exciton dissociation may occur when electrons migrate and were trapped by the Sn-induced potential wells and followed by the holes by Coulomb force. The simultaneous involvement of exciton dissociation with extrinsic exciton trapping may explain for the superlinear increase of PL with excitation power (Figure 2d).[24] To some degree, the emission of such extrinsic self-trapped excitons behaves like that of excitons bound to acceptors or donors, which sometimes also show PL superlinear increase with excitation fluence at the steady state.[62,63] Although the introduction of dopants may reduce the barrier for trapping, we can still find the signature of barrier that PLQY of PEA_2PbI_4:Sn(0.36%) shows its

minimum around 516 nm which coincides with the excitonic absorption peak (Figure S20). It can be interpreted under the framework of the configurational coordination (Figure S21). The intersection between the excitonic branches of PEA_2PbI_4 and Sn traps may result in an energy barrier,[39] so that the excitons with limited kinetic energy (excited at 516 nm) could not easily overcome.

In summary, Sn dopant triggers the occurrence of exciton self-trapping in 2D perovskites where this process is absent in the pure states, resulting in a remarkable red-to-near-infrared emission with luminescence efficiency increase of 8.6 folds at ambient temperature. As revealed by ultrafast transient absorption spectroscopy, Sn-oriented exciton diffusion in the inorganic layer may serve as an essential energy transfer channel, which enables the initial exciton localization which is required for further exciton self-trapping. Given the polar nature of perovskites, it is envisaged that appropriate dopants are likely to facilitate exciton self-trapping cooperatively in perovskites beyond low-dimensional cases. Such success in perovskites would tremendously extend the spectral coverage of perovskites to the short-wavelength infrared regime, and they may find emerging applications in efficient NIR LEDs and supercontinuum sources.

Supporting Information

Supporting Information is available from the Wiley Online Library or from the author.

Acknowledgments

We acknowledge the financial support from Singapore MOE (MOE2014-T2-2-140 and MOE2014-T3-1-004). We also thank the partial financial support from the National Natural Science Foundation of China (No. 51402259), "100 Talents Program" of Fujian Province, the Strategic Priority Research Program of the Chinese Academy of Sciences (XDB20000000), the CAS/SAFEA International Partnership Program for Creative Research Teams, and the International Postdoctoral Exchange Program. J Yu, J Kong and W Hao contributed equally to this work.

Received: ((will be filled in by the editorial staff))
Revised: ((will be filled in by the editorial staff))
Published online: ((will be filled in by the editorial staff))

References

[1] N.-G. Park, M. Grätzel, T. Miyasaka, *Organic-Inorganic Halide Perovskite Photovoltaics*, Springer, Cham 2016.
[2] N.-G. Park, M. Grätzel, T. Miyasaka, K. Zhu, K. Emery, *Nat. Energy* **2016**, 1, 16152.
[3] A. Ummadisingu, L. Steier, J.-Y. Seo, T. Matsui, A. Abate, W. Tress, M. Grätzel, *Nature* **2017**, 545, 208.
[4] C.-H. Chiang, M. K. Nazeeruddin, M. Grätzel, C.-G. Wu, *Energy Environ. Sci.* **2017**, 10, 808.
[5] H. J. Snaith, *Nat. Mater.* **2018**, 17, 372.
[6] L. Dou, Y. Yang, J. You, Z. Hong, W.-H. Chang, G. Li, Y. Yang, *Nat. Commun.* **2014**, 5, 5404.
[7] F. Li, C. Ma, H. Wang, W. Hu, W. Yu, A. D. Sheikh, T. Wu, *Nat. Commun.* **2015**, 6, 8238.
[8] H. Wei, Y. Fang, P. Mulligan, W. Chuirazzi, H.-H. Fang, C. Wang, B. R. Ecker, Y. Gao, M. A. Loi, L. Cao, J. Huang, *Nat. Photon.* **2016**, 10, 333.
[9] Y. C. Kim, K. H. Kim, D.-Y. Son, D.-N. Jeong, J.-Y. Seo, Y. S. Choi, I. T. Han, S. Y. Lee, N.-G. Park, *Nature* **2017**, 550, 87.
[10] G. Xing, N. Mathews, S. S. Lim, N. Yantara, X. Liu, D. Sabba, M. Grätzel, S. Mhaisalkar, T. C. Sum, *Nat. Mater.* **2014**, 13, 476.
[11] H. Zhu, Y. Fu, F. Meng, X. Wu, Z. Gong, Q. Ding, M. V. Gustafsson, M. T. Trinh, S. Jin, X. Y. Zhu, *Nat. Mater.* **2015**, 14, 636.

[12] H. Cho, S.-H. Jeong, M.-H. Park, Y.-H. Kim, C. Wolf, C.-L. Lee, J. H. Heo, A. Sadhanala, N. Myoung, S. Yoo, S. H. Im, R. H. Friend, T.-W. Lee, *Science* **2015**, 350, 1222.
[13] Z. Xiao, R. A. Kerner, L. Zhao, N. L. Tran, K. M. Lee, T.-W. Koh, G. D. Scholes, B. P. Rand, *Nat. Photon.* **2017**, 11, 108.
[14] J. Calabrese, N. L. Jones, R. L. Harlow, N. Herron, D. L. Thorn, Y. Wang, *J. Am. Chem. Soc.* **1991**, 113, 2328.
[15] L. Dou, A. B. Wong, Y. Yu, M. Lai, N. Kornienko, S. W. Eaton, A. Fu, C. G. Bischak, J. Ma, T. Ding, N. S. Ginsberg, L.-W. Wang, A. P. Alivisatos, P. Yang, *Science* **2015**, 349, 1518.
[16] S.-T. Ha, C. Shen, J. Zhang, Q. Xiong, *Nat. Photon.* **2015**, 10, 115.
[17] M. Era, S. Morimoto, T. Tsutsui, S. Saito, *Appl. Phys. Lett.* **1994**, 65, 676.
[18] I. Teruya, in *Optical Properties of Low-Dimensional Materials*, World Scientific, 1996, 288.
[19] R. L. Milot, R. J. Sutton, G. E. Eperon, A. A. Haghighirad, J. Martinez Hardigree, L. Miranda, H. J. Snaith, M. B. Johnston, L. M. Herz, *Nano Lett.* **2016**, 16, 7001.
[20] S. Zhang, G. Lanty, J.-S. Lauret, E. Deleporte, P. Audebert, L. Galmiche, *Acta Mater.* **2009**, 57, 3301.
[21] X. Gong, O. Voznyy, A. Jain, W. Liu, R. Sabatini, Z. Piontkowski, G. Walters, G. Bappi, S. Nokhrin, O. Bushuyev, M. Yuan, R. Comin, D. McCamant, S. O. Kelley, E. H. Sargent, *Nat. Mater.* **2018**, 17, 550.
[22] D. B. Mitzi, in *Prog. Inorg. Chem.*, (Ed: K. D. Karlin), John Wiley & Sons, Inc., New York 1999.
[23] Z. Yuan, C. Zhou, Y. Tian, Y. Shu, J. Messier, J. C. Wang, L. J. van de Burgt, K. Kountouriotis, Y. Xin, E. Holt, K. Schanze, R. Clark, T. Siegrist, B. Ma, *Nat. Commun.* **2017**, 8, 14051.
[24] I. Pelant, J. Valenta, *Luminescence Spectroscopy of Semiconductors*, Oxford University Press, Oxford 2012.
[25] S. C. Erwin, L. Zu, M. I. Haftel, A. L. Efros, T. A. Kennedy, D. J. Norris, *Nature* **2005**, 436, 91.
[26] W. Liu, Q. Lin, H. Li, K. Wu, I. Robel, J. M. Pietryga, V. I. Klimov, *J. Am. Chem. Soc.* **2016**, 138, 14954.
[27] G. Huang, C. Wang, S. Xu, S. Zong, J. Lu, Z. Wang, C. Lu, Y. Cui, *Adv. Mater.* **2017**, 29, 1700095.
[28] W. van der Stam, J. J. Geuchies, T. Altantzis, K. H. W. van den Bos, J. D. Meeldijk, S. Van Aert, S. Bals, D. Vanmaekelbergh, C. de Mello Donega, *J. Am. Chem. Soc.* **2017**, 139, 4087.
[29] S. Zou, Y. Liu, J. Li, C. Liu, R. Feng, F. Jiang, Y. Li, J. Song, H. Zeng, M. Hong, X. Chen, *J. Am. Chem. Soc.* **2017**, 139, 11443.
[30] A. Swarnkar, W. J. Mir, A. Nag, *ACS Ener. Lett.* **2018**, 286.
[31] S. Das Adhikari, S. K. Dutta, A. Dutta, A. K. Guria, N. Pradhan, *Angew. Chem. Int. Ed.* **2017**, 56, 8746.
[32] C. C. Stoumpos, C. D. Malliakas, M. G. Kanatzidis, *Inorg. Chem.* **2013**, 52, 9019.

[33] F. Hao, C. C. Stoumpos, R. P. H. Chang, M. G. Kanatzidis, *J. Am. Chem. Soc.* **2014**, 136, 8094.
[34] B. Zhao, M. Abdi-Jalebi, M. Tabachnyk, H. Glass, V. S. Kamboj, W. Nie, A. J. Pearson, Y. Puttisong, K. C. Gödel, H. E. Beere, D. A. Ritchie, A. D. Mohite, S. E. Dutton, R. H. Friend, A. Sadhanala, *Adv. Mater.* **2017**, 29, 1604744.
[35] H.-C. Wang, W. Wang, A.-C. Tang, H.-Y. Tsai, Z. Bao, T. Ihara, N. Yarita, H. Tahara, Y. Kanemitsu, S. Chen, R.-S. Liu, *Angew. Chem. Int. Ed.* **2017**, 56, 13650.
[36] H. He, Q. Yu, H. Li, J. Li, J. Si, Y. Jin, N. Wang, J. Wang, J. He, X. Wang, Y. Zhang, Z. Ye, *Nat. Commun.* **2016**, 7, 10896.
[37] C. Wehrenfennig, M. Liu, H. J. Snaith, M. B. Johnston, L. M. Herz, *J. Phys. Chem. Lett.* **2014**, 5, 1300.
[38] D. Lee, A. Mysyrowicz, A. V. Nurmikko, B. J. Fitzpatrick, *Phys. Rev. Lett.* **1987**, 58, 1475.
[39] K. S. Song, Williams, Richard T., *Self-Trapped Excitons*, Springer, Cham 1993.
[40] H. Lin, C. Zhou, Y. Tian, T. Siegrist, B. Ma, *ACS Ener. Lett.* **2018**, 3, 54.
[41] G. C. Papavassiliou, I. B. Koutselas, A. Terzis, M. H. Whangbo, *Solid State Commun.* **1994**, 91, 695.
[42] J. A. Dean, *Lange's Handbook of Chemistry*, McGraw-Hill, New York 1999.
[43] X. Hong, T. Ishihara, A. V. Nurmikko, *Phys. Rev. B* **1992**, 45, 6961.
[44] X. Hong, T. Ishihara, A. V. Nurmikko, *Solid State Commun.* **1992**, 84, 657.
[45] J.-i. Fujisawa, T. Ishihara, *Phys. Rev. B* **2004**, 70, 205330.
[46] N. Kitazawa, M. Aono, Y. Watanabe, *Mater. Chem. Phys.* **2012**, 134, 875.
[47] W. K. Chong, K. Thirumal, D. Giovanni, T. W. Goh, X. Liu, N. Mathews, S. Mhaisalkar, T. C. Sum, *Phys. Chem. Chem. Phys.* **2016**, 18, 14701.
[48] D. B. Straus, S. Hurtado Parra, N. Iotov, J. Gebhardt, A. M. Rappe, J. E. Subotnik, J. M. Kikkawa, C. R. Kagan, *J. Am. Chem. Soc.* **2016**, 138, 13798.
[49] W. W. Chow, S. W. Koch, *Semiconductor-Laser Fundamentals: Physics of the Gain Materials*, Springer-Verlag, Berlin Heidelberg 1999.
[50] L. Peedikakkandy, P. Bhargava, *RSC Adv.* **2016**, 6, 19857.
[51] X. Wu, M. T. Trinh, D. Niesner, H. Zhu, Z. Norman, J. S. Owen, O. Yaffe, B. J. Kudisch, X. Y. Zhu, *J. Am. Chem. Soc.* **2015**, 137, 2089.
[52] K. Gauthron, J. S. Lauret, L. Doyennette, G. Lanty, A. A. Choueiry, S. J. Zhang, A. Brehier, L. Largeau, O. Mauguin, J. Bloch, E. Deleporte, *Opt. Express* **2010**, 18, 5912.
[53] M. Saba, M. Cadelano, D. Marongiu, F. Chen, V. Sarritzu, N. Sestu, C. Figus, M. Aresti, R. Piras, A. Geddo Lehmann, C. Cannas, A. Musinu, F. Quochi, A. Mura, G. Bongiovanni, *Nat. Commun.* **2014**, 5, 5049.
[54] E. R. Dohner, A. Jaffe, L. R. Bradshaw, H. I. Karunadasa, *J. Am. Chem. Soc.* **2014**, 136, 13154.
[55] L. Mao, Y. Wu, C. C. Stoumpos, M. R. Wasielewski, M. G. Kanatzidis, *J. Am. Chem. Soc.* **2017**.
[56] Q. Fu, D. Lee, A. V. Nurmikko, L. A. Kolodziejski, R. L. Gunshor, *Phys. Rev. B* **1989**, 39, 3173.

[57] Z. Guo, X. Wu, T. Zhu, X. Zhu, L. Huang, *ACS Nano* **2016**, 10, 9992.
[58] J. L. G. Fierro, *Metal Oxides: Chemistry and Applications*, CRC Press, 2005.
[59] T. M. Brenner, D. A. Egger, L. Kronik, G. Hodes, D. Cahen, *Nat. Rev. Mater.* **2016**, 1, 15007.
[60] X. Wu, M. T. Trinh, X. Y. Zhu, *J. Phys. Chem. C* **2015**, 119, 14714.
[61] S. Ahmad, P. K. Kanaujia, H. J. Beeson, A. Abate, F. Deschler, D. Credgington, U. Steiner, G. V. Prakash, J. J. Baumberg, *ACS Appl. Mater. Interfaces* **2015**, 7, 25227.
[62] T. Schmidt, K. Lischka, W. Zulehner, *Phys. Rev. B* **1992**, 45, 8989.
[63] P. Cai, X. Wang, H. J. Seo, X. Yan, *Appl. Phys. Lett.* **2018**, 112, 153901.

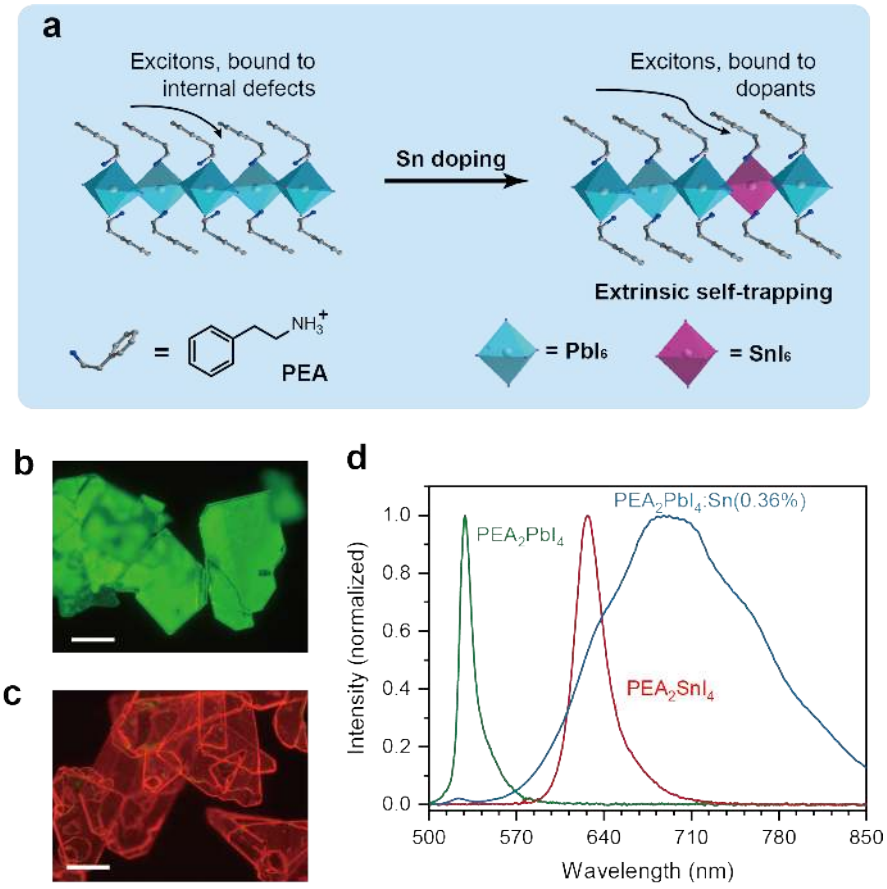

Figure 1. Luminescence properties of 2D perovskites at ambient temperature. (a) Schematic illustration of exciton trapping in pristine and Sn-doped 2D perovskite crystals. Fluorescence micrographs of (b) PEA_2PbI_4 and (c) PEA_2PbI_4:Sn(0.36%) crystals. Scale bar, 100 μm. (d) Microscopic PL emission spectra of bulk crystals taken under a microscope at room temperature. Only the emissions inside the crystals were collected (λ_{ex} = ~470 nm).

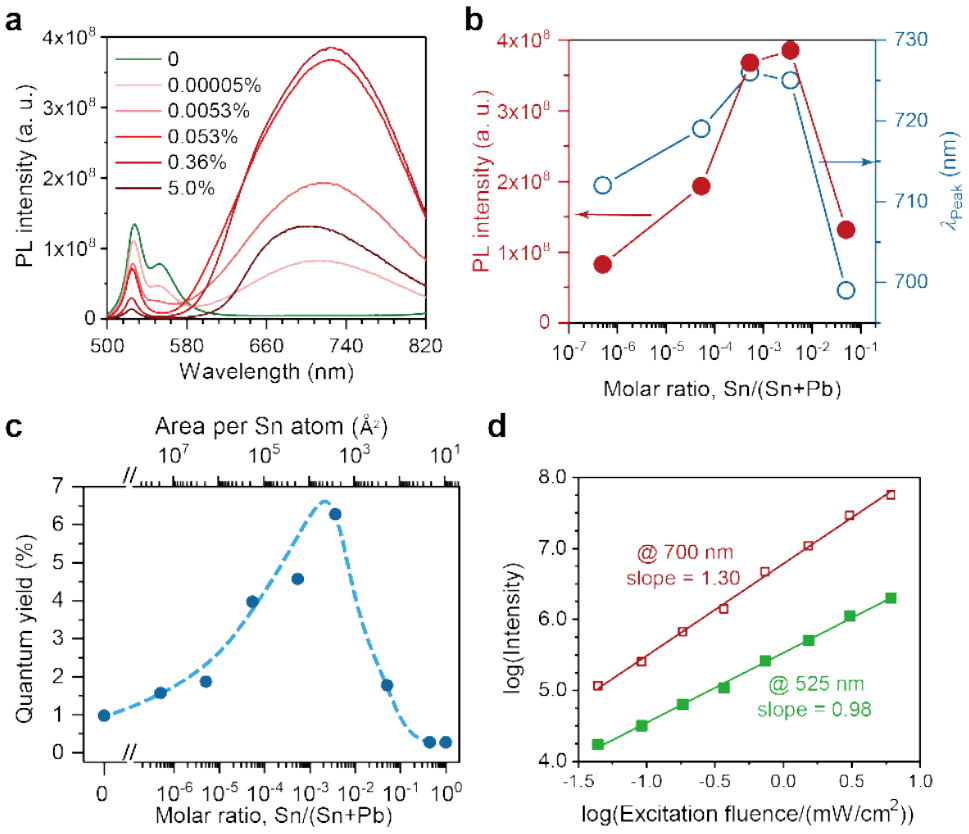

Figure 2. Doping-level-dependent PL properties at room temperature. (a) Emission spectra of PEA_2PbI_4 and Sn-doped PEA_2PbI_4 perovskite crystals, and (b) corresponding intensity and emission peaks as a function of doping levels (λ_{ex} = 470 nm). (c) Quantum yields of perovskite crystals as a function of the molar ratio of Sn and Sn+Pb (λ_{ex} = 472 nm, power density, ~80 μW/cm^2). The dashed line serves as a guide to the eye. (d) Fluence-dependent PL intensity of PEA_2PbI_4:Sn(0.36%) crystals. $R^2_{Adjusted}$ = 0.9971 and 0.9970, respectively, for emission at 525 nm and 700 nm.

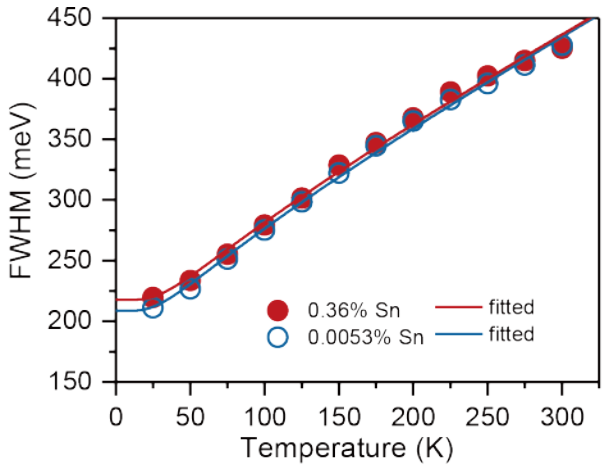

Figure 3. FWHM of PL lines of Sn-doped perovskite crystals as a function of temperature. Data were fitted according to Equation S2 with the fitted parameters of zero-phonon line width Γ_0 = 218 meV, energy of homopolar phonon $\hbar\omega_{HP}$ = 8.8 meV and deformation potential D_{CV} = 7.0×10^8 eV/cm for 0.36%-Sn crystals, and Γ_0 = 209 meV, $\hbar\omega_{HP}$ = 8.0 meV and D_{CV} = 6.6×10^8 eV/cm for 0.0053%-Sn sample.

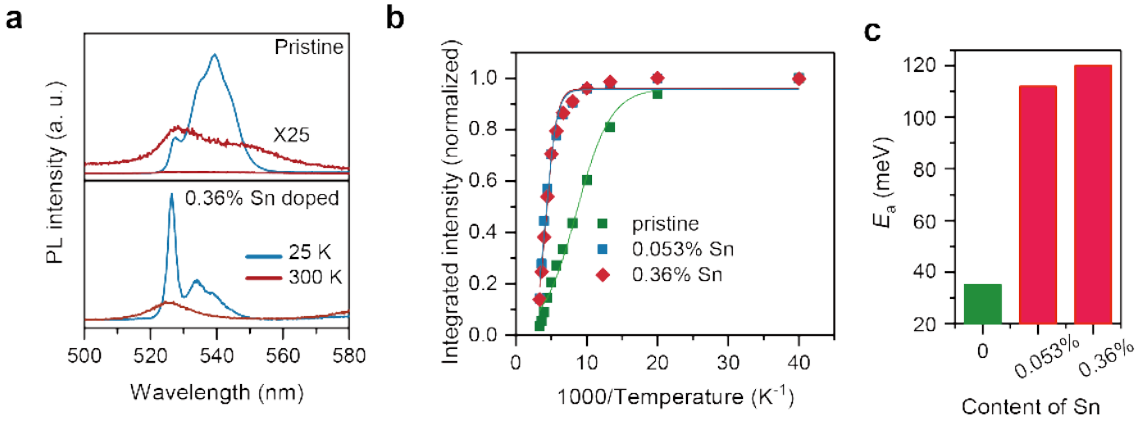

Figure 4. PL quench suppressed by Sn dopants. (a) Temperature-dependent PL spectra of pristine and Sn-doped 2D perovskite crystals (λ_{ex} = 470 nm). (b) Integrated intensity of PL as a function of temperature. Thermal quenching of PL was fitted using the formula of $\eta = I_0/(1+\xi\exp(-E_a/k_BT))$, where E_a is the thermal activation energy for PL quench as plotted in (c), T is the temperature, k_B is Boltzmann constant, and ξ is a parameter associated with radiative and non-radiative recombination times, which are assumed independent of temperature. PL intensity was integrated over 500 to 580 nm for pristine perovskite, and over 560 to 850 nm for Sn-doped samples, as the emissions are negligible in the other spectral regime for corresponding samples.

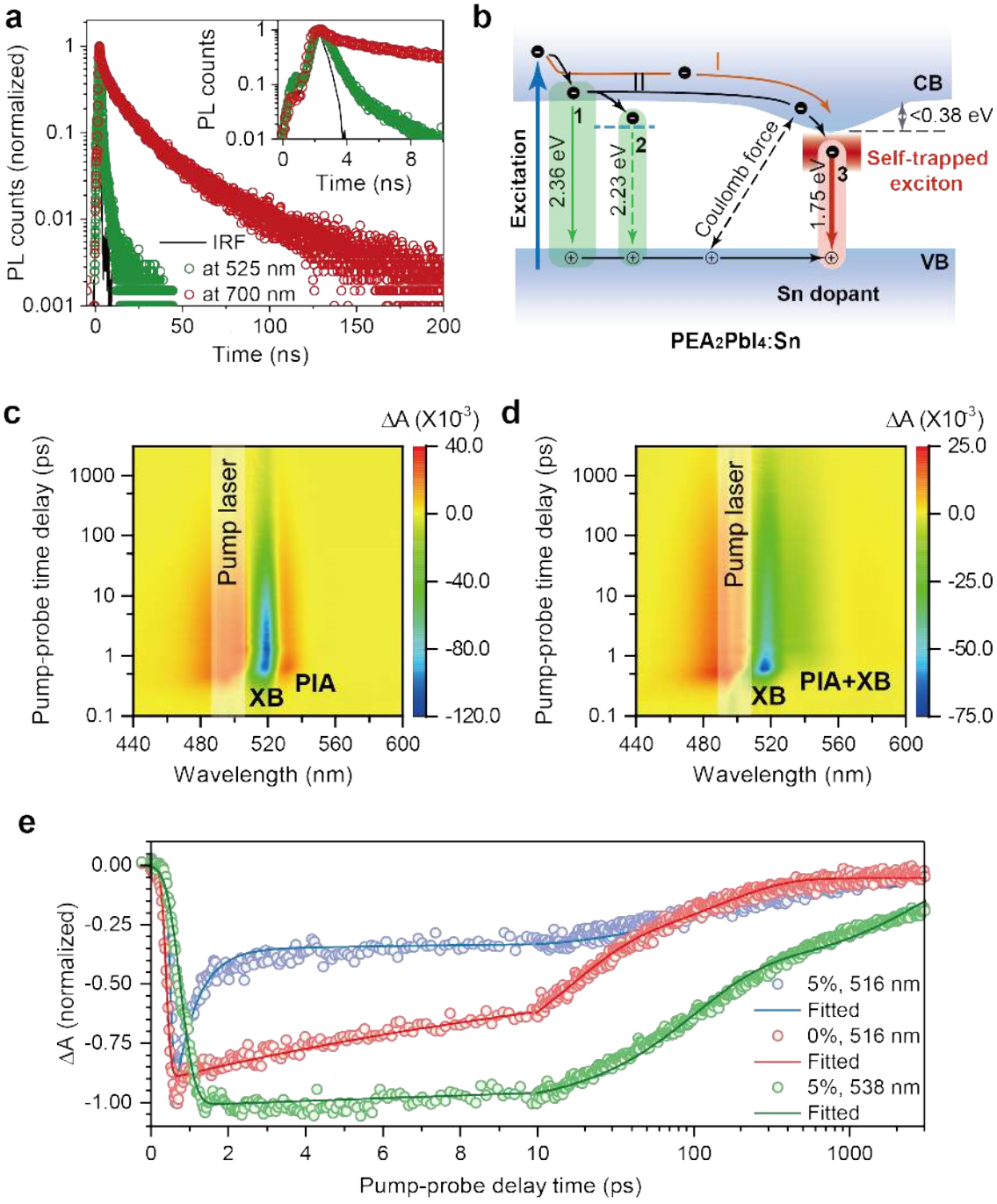

Figure 5. Energy transfer in Sn-doped perovskite films. (a) PL decay curve of 0.36%-Sn-doped 2D perovskite crystals at room temperature and instrumental response (λ_{ex} = 397 nm; pulse duration, ~63 ps; λ_{em} = 525 or 700 nm). IRF, instrument response function. (b) Schematic illustration of radiative channels in Sn-doped 2D perovskites. Arabic numerals 1, 2, and 3 represent the luminescence from

free, bound excitons of pristine perovskite, and Sn-triggered STEs of Sn-doped perovskite, respectively. Roman numerals I and II denote the energy transfer pathway in the form of carrier migration and exciton diffusion, respectively. Pseudo-color (ΔA) representation of transient absorption spectra of pristine (c), and PEA_2PbI_4:Sn(5%) (d) perovskite films. Wavelength of pumping laser, ~495 nm; pulse energy density, ~4 $\mu J/cm^2$. (e) Kinetics of TA signals of pristine and Sn-doped PEA_2PbI_4 films. The data were fitted using a bi-exponential decay model.

The table of contents

Sn dopants trigger extrinsic self-trapping of excitons in bulk 2-dimensional perovskite crystals, and afford broadband red-to-near-infrared emission, with luminescence quantum yield increase from 0.7% to 6.0% (8.6 folds). Random potential wells that Sn dopants create preferentially localize excitons through the fast (sub-picosecond) exciton diffusion so that suppress original weak emissions from free and bound excitons.

Keyword

perovskites, Sn-doping, self-trapped excitons, luminescence, extrinsic

Jiancan Yu, Jintao Kong, Wei Hao, Xintong Guo, Huajun He, Wan Ru Leow, Zhiyuan Liu, Pingqiang Cai, Guodong Qian, Shuzhou Li, Xueyuan Chen,* and Xiaodong Chen*

Broadband extrinsic self-trapped exciton emission in Sn-doped 2-dimensional lead-halide perovskites